Effect of boundary conditions and heat source distribution on temperature distribution in friction stir welding

A. Simar*[1,2], J. Lecomte-Beckers[3], T. Pardoen[2] and B. de Meester[1]

Welding experiments on Al-6005A have been carried out using a fully instrumented milling machine. The power input was calculated from the measured torque and forces. The thermal cycles were measured at various locations close to the weld centreline. A finite element pseudo-steady-state uncoupled thermal model was developed, taking into account the influence of the welding parameters on the power input. The distribution of the total power input between surface and volume heat sources was also studied. The measured and predicted thermal cycles are in good agreement when proper contact conditions between the workpiece and the backing plate are introduced.

Keywords: Friction stir welding, Modelling, Thermal history, Power input

Introduction

Friction stir welding (FSW) is a solid state welding technique, patented by TWI in 1991.[1] The high quality of the welds produced and the reproducibility of this fully automated process have provided the impetus for many industries to use it in production.[2] Nevertheless, many aspects of the process are still poorly understood and require further study, e.g. the temperature field in the nugget and side regions.

The object of the present study is to investigate the effect of the contact conditions between the workpiece and the backing plate and the heat source distribution on the temperature distribution during welding.

After a literature survey of friction stir welding process modelling, the paper will present the experimental method and results of the measurements of the temperature field, forces and torque for various welding parameter values. The finite element model is presented in the next section. It is first identified and analysed by comparison with a single set of experimental data. This is followed by a validation of the identified model parameters for other welding conditions.

Background

The heat in friction stir welding is generated by the frictional effect and/or by plastic deformation associated with material stirring. No consensus has emerged yet as to the proper partitioning of these effects. It is not even clear which is the dominant heat generation mechanism. By using a rather low value for the friction coefficient, Zahedul *et al.*[3] conclude that a purely frictional heating model is probably not adequate. Khandkar *et al.*[4] took the measured mechanical power as input to a FSW thermal model with surface heat sources distributed by assuming a uniform shear stress at the tool interfaces. Tang *et al.*[5] measured the temperatures in the near pin region. The isothermal plateau near the pin suggests that heat is generated mainly through plastic deformation during the friction stir welding process.

The problem of distributing the heat sources around the tool has also been addressed in the literature. Schmidt *et al.*[6] studied the influence of tool shape on the relative amount of heat generated at the tool interface. Schmidt and Hattel[7] applied this proportion to the prediction of the thermal cycles in FSW. Their model includes material convection by the introduction of a simple model for the velocity field. Shi *et al.*[8] distributed a total power input of 1600 W (obtained from the measured torque) between a surface heat source at the shoulder interface (75% of the total power input) and a volume heat source inside the pin (25% of the total power input). McClure *et al.*[9] proposed to reduce the contribution of the pin to 20% of the total power input in an application to thinner sheets. Temperature measurements by Tang *et al.*[5] with a pinless tool gave only a 4% reduction in the maximal temperature measured. They concluded that the pin has a minor influence on the heat input.

The fact that friction stir welding is a solid-state welding process is generally accepted and is sometimes artificially taken into account in models. Frigaard *et al.*[10] limited the maximal temperature of their model to a value close to the eutectic temperature of the alloys studied by adapting the coefficient of friction to prevent the maximal temperature being passed. Song and Kovacevic[11] set the heat input of their model to zero when the melting temperature was reached.

[1]Université Catholique de Louvain, Unité PRM, Place du Levant 2, 1348 Louvain-la-Neuve, Belgium
[2]Université Catholique de Louvain, Department of Materials Sciences and Processes, IMAP, Place Sainte Barbe 2, 1348 Louvain-la-Neuve, Belgium
[3]Université de Liège, Départ. ASMA, IMGC, Bat B52/3, Chemin des Chevreuils 1, Sart Tilman, 4000 Liège, Belgium

*Corresponding author, email simar@prm.ucl.ac.be

Published by Maney on behalf of the Institute
Received 2 September 2005; accepted 16 November 2005
DOI 10.1179/174329306X84409

Table 1 6005A sheet chemical composition

	Alloying element							
	Al	Si	Fe	Cu	Mn	Mg	Cr	Zn	Ti
Weight %	98·39	0·61	0·25	0·09	0·13	0·49	0·020	0·010	0·014

The loss of heat through the contact interface between the bottom of the workpiece and the backing plate has been introduced in numerical models in different ways. Chao and Qi[12] proposed a value of 200 W m^{-2} K^{-1} for the bottom convection coefficient by comparing the results of their 3D finite element model to the experimental results by McClure *et al.*[13] on 6061-T6 aluminium alloy. Fourment *et al.*[14] proposed a similar value for the bottom convection coefficient. Zahedul *et al.*[3] compared four different bottom convection coefficients and concluded that too high a value for this coefficient (4000 W m^{-2} K^{-1}) leads to underestimating the maximum temperature but that an adiabatic condition (0 W m^{-2} K^{-1}) gives maximum temperatures far above the melting point. An intermediate value of 1000 W m^{-2} K^{-1} was therefore chosen. Ulysse[15] did not include the backing plate assuming simply adiabatic conditions at the workpiece/backing plate interface.

Some authors introduced a backing plate in the model and simulated the contact conditions between the workpiece and the backing plate. Colegrove *et al.*[16] proposed a contact conductance of 1000 W m^{-2} K^{-1} between the workpiece and the backing plate. The bottom of the backing plate was set to a temperature of 300 K. In another paper, Colegrove and Shercliff[17] proposed to keep the same contact conductance over the whole interface surface except under the tool region where a perfect contact is introduced. Khandkar *et al.*[4] introduced an annular distribution of the contact conductance that simulates the heat loss in the backing plate. The contact between the workpiece and the backing plate in front of the tool is probably not complete as a result of the backwards inclination of the tool. Shi *et al.*[8] proposed a temperature-dependent contact conductivity between the workpiece and the backing plate. De Vuyst *et al.*[18] showed that such a variation of the contact conductance with temperature ensures a good correlation between experimental and modelling time–temperature curves for the friction stir welded 6005A-T6 and 2024-T3 aluminium alloys.

More complex models include material flow. Bendzsak *et al.*,[19] Shercliff and Colegrove,[20] Seidel and Reynolds,[21] and Colegrove and Shercliff[17,22,23] have developed computational fluid dynamics models to study the material flow assuming the heat input to be due to viscous dissipation. Ulysse,[15] Askari *et al.*,[24] Schmidt and Hattel,[25] Fourment *et al.*[14] and Heurtier[26] developed coupled thermomechanical models which provide an excellent insight into the material flow during the process.

Some models in the literature include residual stress predictions (e.g. Shi *et al.*,[8] Chen and Kovacevic[27]). They are generally based on uncoupled thermal and mechanical models.

Experimental

Samples and FSW apparatus

Butt-welds of 6005A-T6 extruded aluminium sheets were performed. The chemical composition of the alloy is given in Table 1. The plates were 6 mm thick, 90 mm wide and 590 mm long. The welds were 550 mm long. The tool had a 20 mm diameter shoulder and a 7 mm diameter threaded pin. The pin was 5·7 mm long.

The plates were rigidly clamped onto an 80 mm thick, 450 mm wide and 630 mm long steel backing plate. The welding experiments were performed using a Hermle three-axis CNC milling machine (UWF 1001 H) with displacement control.

Measurements during welding

The forces in the three directions of space (F_x, F_y and F_z) as well as the torque M_z (along the tool axis) were measured using a rotating Kistler 9124A dynamometer adapted to the welding head just above the FSW tool.

Type K Thermo-Electric MTS-56050 thermocouples (0·5 mm in diameter) were embedded into the workpiece on the advancing and the retreating sides and within the backing plate. The locations of the thermocouples are provided in Table 2. Note that thermocouples 7 to 10 were located under the tool shoulder. Two additional thermocouples were also inserted into the tool axis, respectively 3 and 13 mm above its shoulder.

Experimental results for various welding conditions

A summary of the experimental results for the welding conditions studied in the paper are presented in Table 3. By repeating experiment number '4' four times, the maximum deviation from the mean of the measured maximum temperature was found to be equal to 7°C. A similar level of deviation also applies to the temperatures measured in the tool. The maximum deviation on the torque M_z was 0·4 N m. Measurements of the transverse

Table 2 Positions of thermocouples

Thermocouple number	Distance from start (centre of tool), mm	Distance to the weld centreline, mm	Depth below the surface, mm	Side: A, advancing; R, retreating
1	430	20	3	A
2	430	16	3	A
3	440	14	3	A
4	430	12	5	A
5	440	12	3	A
6	440	12	3	R
7	420	9·2	2·83	A
8	420	9·2	2·83	R
9	410	7·2	3·3	A
10	410	7·2	3·3	R
11	420	0	7	Within the backing plate

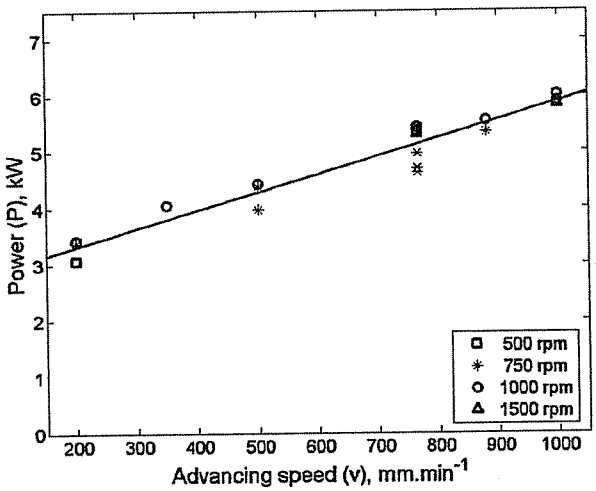

1 Variation of total mechanical power input as a function of advancing speed for different rotational speeds

force F_y and the force in the welding direction F_x never varied by more than 5 kg. The measurement of the vertical force F_z varied more, up to 52 kg. This higher value is because the FSW equipment used is displacement-controlled and not force-controlled. The last experiment (number '5') was also repeated three times and similar maximum deviations were observed.

The total power input is inferred from the torque measurements [$P = M_z.\omega$ where P is the total power (W), M_z is the torque (N m) and ω is the rotational speed (rad s^{-1})]. The experimental data show that the contribution of the force F_x in the welding direction to the total power is negligible.

Figure 1 shows the variation of the total mechanical power input with the welding parameters. The total power input is influenced more by the advancing speed than by the rotational speed. A higher rotational speed corresponds to a slightly higher total power input P. In the range of process parameters tested in the present study, the variation of P with respect to the advancing speed is almost linear. The power input as a function of the advancing speed is fitted with a linear regression based on more experimental results than those presented in Table 3

$$P\,(\mathrm{kW}) \cong 2{\cdot}66 + 0{\cdot}00322v\,(\mathrm{mm\ min^{-1}}) \quad (1)$$

The literature is not clear as to the dependence of the advancing and rotational speeds on the power input. Tang *et al.*[5] interpreted temperature measurements on 6061-T6 aluminium alloy welds (60 mm min^{-1} welding speed) by concluding that with a higher rotational speed, temperature should increase but that increasing temperature should reduce the material flow stress which in turn limits the power generation and temperature increases. Colegrove and Shercliff[28] concluded from temperature measurements on 16 mm thick welds of 7075 aluminium alloy that the maximum temperature was close to the solidus temperature and therefore that heat generation was limited, which gives a weld power independent of the rotational speed. They also suggested that the power input is proportional to the square root of the advancing speed. On the other hand, Record *et al.*[29] concluded from a statistical study on 7075 aluminium alloy welds that the power input is influenced by both the rotational and the advancing speed.

From the literature, it can be concluded that the material being welded and the process parameters influence the effect of the rotational speed on the power input. In hot welds, the power input seems to be relatively independent of the rotational speed. Experimental results from the present study concern rather hot welds which might explain the small influence of the rotational speed on the power input.

Temperature measurements at two locations along the tool axis allow a simple evaluation of the heat losses into the tool (Q_{tool}).[30] An estimate of the welding efficiency is obtained by subtracting the heat loss from the total power input

$$\eta = \frac{P - Q_{tool}}{P} \quad (2)$$

Table 3 Summary of experimental results

	Experiment				
	1	2	3	4	5
Advancing speed, mm min^{-1}	200	200	200	765	1000
Rotational speed, rev min^{-1}	500	750	1000	1000	1000
T1 max, °C	255	263	268	200	181
T2 max, °C	302	312	316	244	222
T3 max, °C	336	344	349	279	259
T4 max, °C	368	374	379	310	298
T5 max, °C	371	380	391	322	298
T6 max, °C	386	409	425	316	294
T7 max, °C	432	444	457	409	395
T8 max, °C	421	447	467	385	346
T9 max, °C	437	452	465	413	398
T10 max, °C	437	465	484	411	383
T11 max, °C	310	333	350	247	225
Force F_x in the transverse direction, kg	57	38	39	61	89
Force F_y in the welding direction, kg	32	29	48	143	223
Vertical force F_z, kg	953	1073	1137	1574	1687
Torque M_z, N m	58·6	43	32·7	51·1	56·3
Power, kW	3·07	3·38	3·42	5·35	5·9
Tmax in tool 3 mm from shoulder, °C	489	536	544	522	502
Tmax in tool 13 mm from shoulder, °C	371	408	421	345	310

This efficiency is only weakly affected by the welding parameters and is equal to 95%.

The value of the heat loss into the tool has also been studied in the literature, leading to similar conclusions: Chao *et al.*[31] and Dickerson *et al.*,[32] after modelling the temperature distribution in the tool and comparing it to experiments, conclude that the heat loss is about 5%. Dickerson *et al.* give a value of 10% under steady-state conditions. Many other authors use process efficiencies of about 90%.[8,25]

Measurements of properties of aluminium alloy 6005A-T6

Measurements of the thermal properties of aluminium alloy 6005A-T6 with temperature have been performed (Table 4). Three types of measurements up to 550°C were performed twice to obtain those properties.

(i) A measurement of the dilation response performed with a DIL 402C dilatometer in order to calculate the density at various temperatures.

(ii) DSC (differential scanning calorimetry) measurement (heating and cooling up to 550°C) performed with STA 449C equipment in order to calculate the evolution of the 'true' specific heat with temperature by subtracting the effects of phase transformations. The average value between the heating and the cooling phases was retained.

(iii) A Laser-Flash measurement performed with LFA 427 equipment providing the evolution of the thermal diffusivity with temperature. The evolution of the thermal conductivity with temperature is obtained by multiplying the information on the thermal diffusivity by the density and specific heat of the alloy.

DSC measurements up to the melting point were performed in order to estimate the solidus and liquidus temperatures of the alloy. In the heating phase, the solidus was found at 613°C and the liquidus at 704°C. In the cooling phase, the liquidus was detected at 651°C and the solidus at 566°C. Note that the DSC measurements were performed at 10 K min^{-1}. This heating rate is much lower than the typical rates measured during welding which could cause a delay in the appearance of a new phase.

The mechanical properties of the alloy were measured at room temperature and are presented in Table 5.

Table 5 Mechanical properties of Al-6005A-T6 alloy

Young's Modulus, GPa	75
Yield strength, MPa	252
Tensile strength, MPa	272
Elongation, %	35

Description of model

General assumptions

A finite element model of the pseudo-steady-state heat transfer during welding was developed using the general purpose commercial code ABAQUS.[33] The mesh is made up of hexahedrons with a high density in the near tool region. The model is sufficiently long that it does not influence the thermal field around the tool.

A temperature of 25°C was imposed upstream. The top and side surfaces were considered as adiabatic. The effect of convection at these surfaces on the temperature distribution is indeed negligible. The model takes into account the heat loss through the backing plate by modelling a thick steel plate under the workpiece. A temperature of 25°C was imposed at the bottom of this thick steel plate. The contact conditions between the workpiece and the thick steel plate will be detailed later.

In order to avoid discontinuities in the flow field of aluminium, the pin was ignored. Taking the steel pin into account would require to model the way the aluminium bypasses the pin since the pin does not advance with the material.

Heat dissipated by friction at tool/workpiece interface – surface heat sources

One may divide the total power dissipated at the tool/workpiece interface by friction (surface heat sources) into three parts corresponding to the various working surfaces of the tool: the shoulder (radius r_o), the lateral surface of the pin (radius r_i and height h_p) and the surface of the tool pin tip. The purely sliding friction effect of the shoulder due to the advancing speed can be neglected compared to the rotating terms of friction (Shercliff and Colegrove[20]). Similarly, the heat generated at the tool tip can be neglected compared to the heat generated along the shoulder and the pin lateral surface. The relative proportions of friction heat dissipated on the shoulder and the pin of the tool are 82% and 18%, respectively, for the tool geometry of interest in the present study.[30] The surface heat sources

Table 4 Thermal properties of Al-6005A-T6 alloy versus temperature

Temperature, °C	Density ρ, kg m^{-3}	Specific heat C_p, J kg^{-1} K^{-1}	Thermal conductivity λ, W m^{-1} K^{-1}
25	2680	...	
50	2680	920	206·6
100	2670	930	208·3
150	2660	950	210·3
200	2650	970	210·3
250	2630	990	210·9
300	2620	1010	208·6
350	2610	1020	205·6
400	2600	1040	201·9
450	2590	1060	197·5
500	2580	1080	190·0
550	...	1110	182·8

[q_S (W m^{-2})] are related to the total power input associated with surface heat sources [Q_S (W)],[30] along the tool shoulder by

$$q_S = \frac{0{\cdot}82 Q_S r}{\frac{2}{3}\pi\left(r_o^3 - r_i^3\right)} \text{ with } r_0 \leqslant r \leqslant r_i \text{ and } z = 0 \quad (3)$$

and along the lateral surface of the tool pin by

$$q_S = \frac{0{\cdot}18 Q_S}{2\pi r_i h_p} \quad \text{with } 0 \leqslant z \leqslant h_p \text{ and } r = r_i \quad (4)$$

Heat dissipated by material stirring (plastic deformation) – volume heat sources

Heat is also dissipated in the volume of the material by plastic deformation. The corresponding volume heat sources are equal to

$$q_V = \beta \dot{\varepsilon}_{ij}^p \sigma_{ij} \text{ (W m}^{-3}\text{)} \quad (5)$$

where $\dot{\varepsilon}_{ij}^p$ and σ_{ij} are the components of the plastic strain rate tensor and the Cauchy stress tensor, respectively and β is a parameter ranging typically[34] between 0·8 and 0·99 that accounts for the fact that a small part of the energy is stored in the material in the form of defects. Several research teams (Heurtier-Monteillet, Deepweld project, etc.) are currently developing models to numerically simulate the plastic flow and accompanying heat generation. The problem is extremely complex not only because the flow is complex but also because the constitutive relationships are complex. Indeed, the isoplastic response depends on rate and temperature dependent internal variables characterising the hardening and softening behaviour associated with the microstructural evolution (precipitate dissolution, recrystallisation, recovery).

A purely phenomenological approach is used in the present study. Little can be predicted concerning the location and intensity of the heat dissipation through plastic deformation during FSW, except that it occurs in the so-called thermomechanically affected zone (TMAZ) as is experimentally confirmed and agreed upon in the literature. Dong *et al.*[35] concluded from their models that plastic slip at the surface due to mechanical interactions between the tool and the base material seems to correlate with the friction-stir weld profile obtained by macrographs. The inverse model of Lambrakos *et al.*[36] allowed them to conclude that there is a strong correlation between the physical shape of the stirred region and the volume distribution of heat generated by the stirring process. The thermomechanical model of Askari *et al.*[24] shows that the deformed region is confined to the area immediately surrounding the pin and under the shoulder. The deformation of the material is very large close to the FWS tool but, due to heating, the flow stress there is the lowest. Conversely, away from the tool, the deformation is lower but the material flow stress is higher because the temperatures are lower.

In the absence of any other relevant information, a uniform distribution of the volume heat sources resulting from the plastic deformation in the TMAZ will be assumed. The total heat power dissipated through plastic deformation is proposed to be

$$Q_V = q_V V_p \quad (6)$$

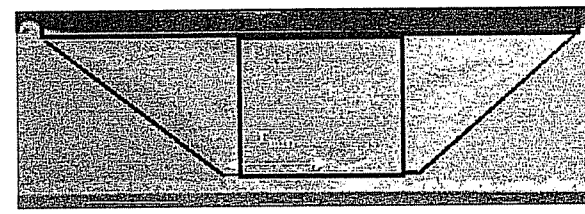

2 Shape of TMAZ

where V_p (m^3) is the volume of the TMAZ and Q_V (W) is the volume heat source power.

From macrographic observations on a transverse section, the volume V_p of the TMAZ where plastic deformation takes place during FSW has been determined as shown in Fig. 2. The advantage of choosing this very simple description of the shape of the TMAZ avoids the need to prepare a macrograph of the weld in order to use the model.

The value of r_{min} (defined in Fig. 2) seems to depend mainly on the advancing speed and was measured as $r_i + 0{\cdot}5$ mm = 4 mm for experiments 4 and 5 (765 and 1000 mm min^{-1}, respectively) and $r_i + 3{\cdot}5$ mm = 7 mm for experiments with a lower welding speed (200 mm min^{-1}).

Colegrove and Shercliff[28] drew similar conclusions from their macrosection observations. In their experiments, the size of the TMAZ diminishes if the welding speed increases but the rotational speed had no influence on the nugget size.

Distribution of mechanical power between surface and volume heat sources

The total power dissipated by friction and plastic deformation during welding can be calculated from the measurements of the force and torque. Almost all that power is transformed into heat. As explained above, the energy stored in the material in the form of dislocations and other microstructural defects such as new grain boundaries for instance is very small. The portion of the power lost within the tool is very small

$$\eta P = P_{in} = Q_S + Q_V \quad (7)$$

The relative importance of Q_V and Q_S is unknown. In the present study, the parameter γ is introduced for that purpose

$$Q_V = \gamma P_{in} \quad (8)$$

$$Q_S = (1-\gamma) P_{in} \quad (9)$$

Contact conditions between workpiece and backing plate

The contact conditions between the workpiece and the backing plate must be carefully described when modelling. Many authors have shown that various options can be considered.

(i) Case 1: No backing plate. In that situation, the lower surface of the workpiece is assumed to be adiabatic. This case would be representative of a very poor contact between the workpiece and the backing plate.

(ii) Case 2: Perfect contact between workpiece and backing plate.

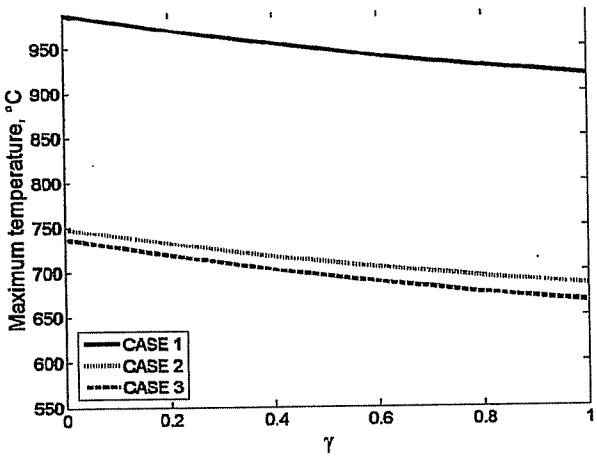

3 γ versus maximum temperature for various contact conditions

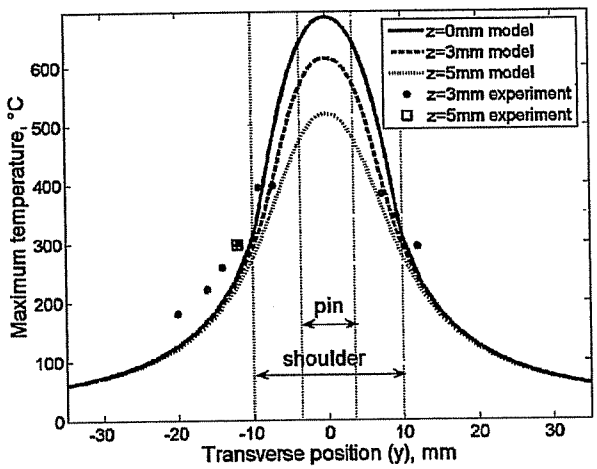

4 Variation of maximum temperature versus distance to centreline for 'Case 2' with γ=1 and r_{min}=4 mm

(iii) Case 3: Perfect contact under the tool region only. The contact under the tool is chosen to be a perfect aluminium/steel contact. This case is suggested by experimental observations: the high pressures under the tool lead to a visible indentation of the upper surface of the backing plate along a width approximately equal to the diameter of the tool. There, the contact is certainly extremely good. In the surrounding area, the quality of the contact decreases when moving away from the centreline but it is difficult to quantify its evolution. A thermal contact conductance was thus introduced between the aluminium sheets and the backing plate. This contact condition is imposed in the FE code by artificially introducing a material layer of 0·2 mm thickness with a thermal conductivity equal to that of steel multiplied by a factor called α. The corresponding contact conductivity thus reads

$$CC=\frac{\alpha\lambda}{t}=\frac{\alpha\cdot 47\ (\mathrm{W\,m^{-1}\,K^{-1}})}{0{\cdot}2\ (\mathrm{mm})}$$
$$=\alpha\cdot 235\ (\mathrm{kW\,m^{-2}\,K^{-1}}) \qquad (10)$$

where λ is the thermal conductivity of steel, t is the thickness of the layer, and α is equal to 1 under the tool, lower than 1 behind the tool and equal to 0 elsewhere.

Modelling results and discussion

A comparison of the influence of the various parameters of the model, i.e. (i) γ which partitions the importance of surface and volume heat sources and (ii) the type of contact between the workpiece and the backing plate, in the various contact workpiece/backing plate conditions, will first be made for a single set of experimental parameters (1000 rev min^{-1} and 1000 mm min^{-1}, i.e. experiment '5').

Maximum temperature

Figure 3 compares the maximum temperatures reached under the shoulder behind the pin. Case 1 leads to unrealistic predictions with temperatures far above the liquidus. The other cases have little influence on the maximum temperature and provide more reasonable values for the maximum temperature.

When parameter γ increases, i.e. the volumetric proportion of the heat source increases, the maximum temperature reached decreases. Considering only the maximum temperature, γ=1 (only volume heat sources) seems to be the most realistic choice since maximum temperatures in FSW should be below the solidus of the material. Since heating rates are much higher in FSW, the effective solidus temperature will be higher than the 613°C measured by DSC at 10 K min^{-1}. On the other hand, the influence of the material flow around the tool is not taken into account, which would reduce the maximum temperature due to the stirring of hot material. Indeed, even though aluminium has a high thermal conductivity, heat convection in the stirred zone has a considerable effect on the maximum temperature obtained.[37]

Chao and colleagues[12,31] assumed a frictional heat source with a fitted total power input of 1·4 kW. The welding parameters were a rotational speed of 400 rev min^{-1} and an advancing speed of 120 mm min^{-1}. Their 6061-T6 aluminium alloy plates were 6·4 mm thick. For similar welding parameters, the power input measured in the present study is much higher, about 3 kW. The very low value of the fitted power input reported in their article confirms that a purely surface heat source is probably not adequate either.

Cooling rates

The contact resistance of Case 2 does not give satisfactory results for the maximum temperatures reached away from the centreline (Fig. 4). Note that these maximum temperatures are not reached at the same time for various y positions.

The contact condition for Case 3 with α=0 behind the tool accurately reproduces the maximum temperature away from the centreline (Fig. 5). The cooling rates are, however, underestimated (Fig. 6). This effect can be corrected using a small contact resistance in the regions surrounding the tool.

On the basis of the aforementioned observations, it is suggested to select a value of α behind the tool that minimises the difference between the predicted and

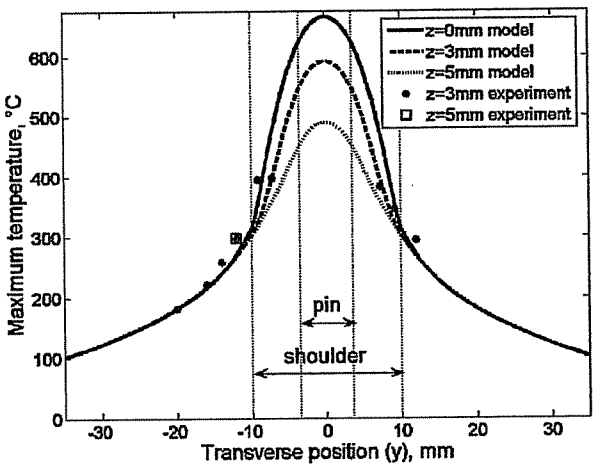

5 Variation of maximum temperature versus distance to centreline (y>0 on R side) for 'Case 3' with α=0, γ=1 and r_{min}=4 mm

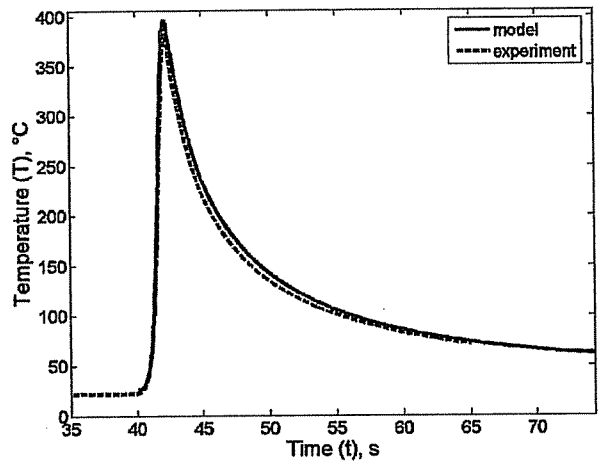

7 Variation of temperature versus time for thermocouple 10 (y=7·2 mm) for 'Case 3' with α=0·0075, γ=1 and r_{min}=4 mm

measured temperatures at the end of the plate, i.e. 60 mm away from the tool centre. Choosing α=0·0075 minimises that error.

Figure 7 shows the results of modelling with α= 0·0075 and γ =1. The temperatures in the aluminium sheet are well predicted at various distances from the weld centreline and at various depths giving results similar to those of Fig. 5. Figure 7 shows the good prediction of the cooling rate with such a value of α.

Choosing α=0·0075 leads to a contact conductivity behind the tool equal to 1·76 kW m^{-2} K^{-1}. Shi *et al.*[8] also proposed a similar value for the contact conductivity for temperatures below 150°C. Khandkar *et al.*[4] used a contact conductivity between the workpiece and the backing plate equal to 10 kW m^{-2} K^{-1} in front of the tool and 100 kW m^{-2} K^{-1} to the rear of the tool. They also introduced a contact conductivity between the workpiece and the backing plate equal to 1 kW m^{-2} K^{-1} in the other regions. The choice made in the present study is very similar, i.e. a contact conductivity equal to 1·76 kW m^{-2} K^{-1} behind the tool and 0 kW m^{-2} K^{-1} elsewhere except under the tool where a much higher value is taken but without distinguishing between the front and the back of the tool.

Assessment of model for other welding parameters

For the sake of validation, the model has been applied to other welding conditions with the values α and γ identified by experiment '5'. Figures 8 and 9 show that the model provides very good predictions of the maximum temperature for all the welding parameters proposed in Table 3. Even though these welding parameters are quite different from those used for the calibration of α and γ, the predictions only slightly underestimate the experimental data, this effect being more noticeable further away from the centreline. The cooling rate is always well predicted.

Conclusions

A finite element model of the friction stir welding process has been developed and validated based on fully instrumented, reproducible Al-6005A-T6 welding experiments. The most important empirical parameter of the model is the total power input. This is influenced mainly by the advancing speed. An empirical formula

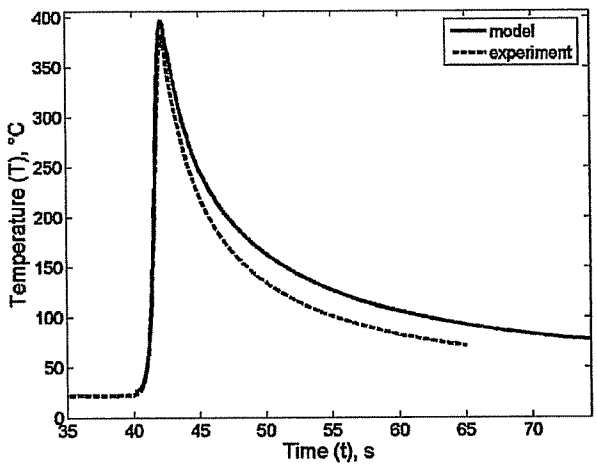

6 Variation of temperature versus time for thermocouple 10 (y=7·2 mm) for 'Case 3' with α=0, γ=1 and r_{min}=4 mm

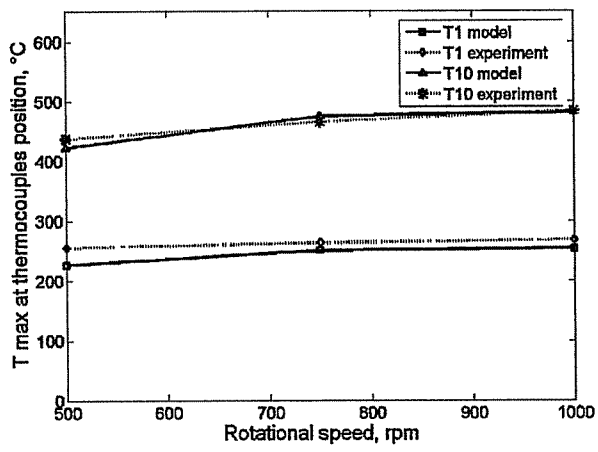

8 Effect of rotational speed on maximum temperature measured by thermocouples 1 and 10 for an advancing speed of 200 mm min^{-1}

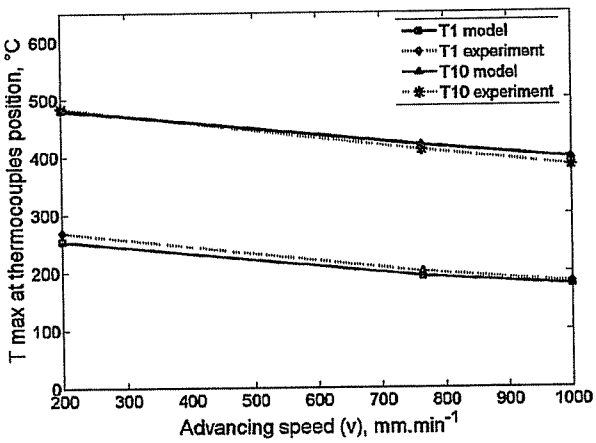

9 Effect of advancing speed on maximum temperature measured by thermocouples 1 and 10 for rotational speed of 1000 rev min^{-1}

for the determination of the total power input is suggested in order to be able to apply the model in a predictive way. The other 'free' parameters of the model have been identified based on the experimental measurements of the present study, i.e. (i) the proportion of heat associated with surface and volume heat sources, (ii) the contact condition between the workpiece and the backing plate.

The following conclusions were derived from the identification procedure.

1. Surface heat sources lead to unrealistically high maximum temperatures. Hence, heat dissipation due to contact between the tool and the aluminium does not seem to be confined to the tool surface.

2. Volume heat sources uniformly distributed over the TMAZ give reasonable predictions for the maximum temperature.

3. The contact conditions between the workpiece and the backing plate must depend on the distance to the tool. Perfect contact under the tool, combined with a contact conductivity of only 0·75% of that value behind the tool and equal to 0 everywhere else, provides excellent predictions of the cooling rates. Nevertheless, the reliability of the contact conductivity parameters could be increased by appropriate experimental measurements.

Acknowledgements

Aude Simar acknowledges the financial support from FRIA and FSR-UCL. The authors are grateful to SAPA RC Profil Ghlin S.A. for providing the aluminium sheets. The authors also acknowledge the support of the technical staff of PRM, TERM, IMAP and IMGC in the experimental work.

References

1. M. W. Thomas, E. D. Nicholas, J. C. Needham, M. G. Murch, P. Templesmith and C. J. Dawes: GB Patent Application No. 9125978·8, December 1991; US Patent No. 5460317, October 1995.
2. D. E. Nicholas and S. W. Kallee: Proc. 'Lassen van aluminium' study day, De Nayer Instituut, Belgium, October 2002.
3. M. Zahedul, H. Khandkar and J. A. Khan: *J. Mater. Process. Manuf. Sci.*, 2001, **10**, 91–105.
4. M. Z. H. Khandkar, J. A. Khan and A. P. Reynolds: *Sci. Technol. Weld. Joining*, 2003, **8**, 165–174.
5. W. Tang, X. Guo, J. C. McClure and L. E. Murr: *J. Mater. Process. Manuf. Sci.*, 1998, **7**, 163–172.
6. H. Schmidt, J. Hattel and J. Wert: *Modell. Simul. Mater. Sci. Eng.*, 2004, **12**, 143–157.
7. H. Schmidt and J. Hattel: Proc. ISOPE-2004, Toulon, France, 2004, ISOPE, No. 2004-FSW-11.
8. Q. Shi, T. Dickerson and H. R. Shercliff: Proc. 4th Int. Symp. FSW, Park City, Utah, USA, May 2003, TWI (CD ROM).
9. R. W. McClure, H. Ou, C. G. Armstrong and M. Price: Proc. 5th Int. Symp. FSW, Metz, France, Sept. 2005, TWI (CD ROM).
10. O. Frigaard, O. Grong and O. T. Midling: *Metal. Mater. Trans. A*, 2001, **32A**, 1189–1200.
11. M. Song and R. Kovacevic: *Int. J. Mach. Tools Manuf.*, 2003, **43**, 605–615.
12. Y. J. Chao and X. Qi: *J. Mater. Process. Manuf. Sci.*, 1998, **7**, 215–233.
13. J. C. McClure, Z. Feng, T. Tang, J. E. Gould, L. E. Murr and X. Guo: Proc. 5th Int. Conf. 'Trends in welding research', Pine Mountain, GA, USA, June 1998, ASM International, 590–595.
14. L. Fourment, S. Guerdoux, M. Miles and T. Nelson: Proc. 5th Int. Symp. FSW, Metz, France, Sept. 2005, TWI (CD ROM).
15. P. Ulysse: *Int. J. Mach. Tools Manuf.*, 2002, **42**, 1549–1557.
16. P. Colegrove, M. Painter, D. Graham and T. Miller: Proc. 2nd Int. Symp. FSW, Gothenburg, Sweden, June 2000, TWI (CD ROM).
17. P. A. Colegrove and H. R. Shercliff: *Sci. Technol. Weld. Joining*, 2004, **9**, 352–361.
18. T. De Vuyst, L. D'Alvise, A. Simar, B. de Meester and S. Pierret: *Weld. World*, 2005, **49**, 47–55.
19. G. J. Bendzsak, T. H. North and C. B. Smith: Proc. 2nd Int. Symp. FSW, Gothenburg, Sweden, 2000, TWI.
20. H. R. Shercliff and P. A. Colegrove: *Math. Model. Weld. Phenomena*, 2002, **6**, 927–974.
21. T. U. Seidel and A. P. Reynolds: *Sci. Technol. Weld. Joining*, 2003, **8**, 175–183.
22. P. A. Colegrove and H. R. Shercliff: *Sci. Technol. Weld. Joining*, 2004, **9**, 483–492.
23. P. A. Colegrove and H. R. Shercliff: *Sci. Technol. Weld. Joining*, 2004, **9**, 345–351 and 352–361.
24. A. Askari, S. T. Silling, B. London and M. Mahoney: Proc. FSW Visual Model. Seminar, Germany, 2003, GKSS.
25. H. Schmidt and H. Hattel: Proc. 5th Int. Symp. FSW, Metz, France, Sept. 2005, TWI (CD ROM).
26. P. Heurtier: PhD thesis, Ecole Nationale Supérieure des Mines de Saint-Etienne, France.
27. C. M. Chen and R. Kovacevic: *Int. J. Mach. Tools Manuf.*, 2003, **43**, 1319–1326.
28. P. A. Colegrove and H. R. Shercliff: *Sci. Technol. Weld. Joining*, 2003, **8**, 360–368.
29. J. H. Record, J. L. Covington, T. W. Nelson, C. D. Sorensen and B. W. Webb: Proc. 5th Int. Symp. FSW, Metz, France, Sept. 2005, TWI (CD ROM).
30. A. Simar, T. Pardoen and B. de Meester: Proc. 5th Int. Symp. FSW, Metz, France, Sept. 2005, TWI (CD ROM).
31. Y. J. Chao, X. Qi and W. Tang: *Trans. ASME*, 2003, **125**, 138–145.
32. T. Dickerson, Q. Shi and H. R. Shercliff: Proc. 4th Int. Symp. FSW, Park City, Utah, USA, May 2003, TWI (CD ROM).
33. Hibbit, Karlsson and Sorensen: 'ABAQUS, Version 6.3, user's manual'; 2002, Providence, RI, USA.
34. P. Rosakis, A. J. Rosakis, G. Ravichandran and J. Hodowany: *J. Mech. Phys. Solids*, 2000, **48**, 581–607.
35. P. Dong, F. Lu, J. K. Hong and Z. Cao: *Sci. Technol. Weld. Joining*, 2001, **6**, 281–287.
36. S. G. Lambrakos, R. W. Fonda, J. O. Milewski and J. E. Mitchell: *Sci. Technol. Weld. Joining*, 2003, **8**, 385–390.
37. A. Simar, T. Pardoen and B. de Meester: Proc. 7th Int. Conf. 'Trends in welding research', Pine Mountain, GA, USA, May 2005, ASM International.